Interference effects on guided Cherenkov emission in silicon from perpendicular, oblique, and parallel boundaries

M. Couillard,* A. Yurtsever,† and D. A. Muller
School of Applied and Engineering Physics, Cornell University, Ithaca, New York 14850, USA
(Received 7 March 2010; published 18 May 2010)

Waveguide electromagnetic modes excited by swift electrons traversing Si slabs at normal and oblique incidence are analyzed using monochromated electron energy-loss spectroscopy and interpreted using a local dielectric theory that includes relativistic effects. At normal incidence, sharp spectral features in the visible/near-infrared optical domain are directly assigned to *p*-polarized modes. When the specimen is tilted, *s*-polarized modes, which are completely absent at normal incidence, become visible in the loss spectra. In the tilted configuration, the dispersion of *p*-polarized modes is also modified. For tilt angles higher than ~50°, Cherenkov radiation, the phenomenon responsible for the excitation of waveguide modes, is expected to partially escape the silicon slab and the influence of this effect on experimental measurements is discussed. Finally, we find evidence for an interference effect at parallel Si/SiO_2 interfaces, as well as a delocalized excitation of guided Cherenkov modes.

DOI: 10.1103/PhysRevB.81.195315 PACS number(s): 73.20.Mf, 41.60.Bq, 79.20.Uv, 68.37.Lp

I. INTRODUCTION

An electron traveling in a medium at a speed larger than the phase velocity of light in that medium will generate radiation. This phenomenon is known as the Cherenkov effect.[1] Basically, a field wavefront following the incident electron is formed along a cone (similar to shock and bow waves), and radiation is emitted at a characteristic angle θ_c given by $\cos(\theta_c)=1/(\beta n)$, where β is the speed of incident electrons v divided by the speed of light in vacuum c, and n is the refractive index of the medium. For a typical accelerating voltage of 200 keV in a transmission electron microscope (TEM), Cherenkov losses are expected in several technologically important semiconductors and insulators, such as Si and SiO_2. Because the photon energy is taken from the incident electrons, radiative losses will appear in electron energy-loss spectra (EELS), along with more well-known losses associated with interband transitions as well as bulk and interface plasmons.[2]

Usually, Cherenkov losses occur in semiconductors and insulators at energies lower than the optical gap onset, which often prevents the direct measurement of band gap energies by EELS (Refs. 3–7) and poses a particular problem in stratified structures such as gate stacks with thin oxide layers.[8] Cherenkov radiation is a coherent, far-field response of the medium to the passing electron. Dimensions of the probed structure must therefore exceed the so-called formation length for the radiation to be emitted. It is only in small, isolated or ultrathin structures such as suspended nanotubes that direct band-gap measurements can be made reliably.[9] However, when many nanoparticles are located in proximity to each other, Cherenkov emission can again occur if the dielectric function of the effective medium meets the Cherenkov condition.[10]

The geometry of the target structure can strongly affect the expected shape of valence energy-loss spectra.[11–18] A particular example is the formation of waveguide modes in thin slabs of a high-refractive index materials surrounded by low-index media.[19,20] For the particular case of silicon slabs standing in vacuum, strong peaks appear in loss spectra below 3.4 eV and can be directly associated with *p*-polarized guided modes.[10] The origin of these spectral features can be explained in the momentum space, where the continuous dispersion of the Cherenkov mode in a bulk medium[21] is expected to separate into a finite number of guided modes for the case of a slab. Such momentum dispersion for guided modes has previously been observed experimentally for thin graphite films,[22] and these measurements were later compared with simulations based on a dielectric model.[19] By forming a nanometer scale electron probe, it becomes possible to probe radiative losses locally, such as whispering gallery modes of individual nanoparticles[23] and optical modes of photonic crystals.[24] Hence, even if radiative losses partially mask the *electronic* density of states component of the EELS signal, it also reveals information on the *photonic* density of states.[25]

While previous work has focused largely on the momentum space distribution of loss functions in slabs, real space probes provide opportunities to examine the consequences of spatially broken symmetries and finite boundary conditions. This paper presents a monochromated EELS investigation of the influence of the position and the incidence angle of the electron trajectory on the emission of Cherenkov radiation in silicon slabs. We compare experimental results with a local dielectric model that includes retardation effects[26] to identify the various radiative contributions to the loss spectra. For electrons impinging at normal incidence on a Si slabs, *p*-polarized modes (magnetic field parallel to the slab surfaces) are excited and we describe the influence of the slab thickness on the emission probability. As the sample is tilted away from normal incidence, changes in *p*-polarized modes are explained. Also, peaks associated with *s*-polarized modes (electric field parallel to the slab surfaces), which are completely absent at normal incidence, are found to contribute substantially to the experimental spectra. When the tilt angle exceeds a threshold defined by the Cherenkov emission angle and the condition for total internal reflection, some radiation escapes the silicon slab resulting in a modification

of the loss signal. Finally, we consider the emission of guided modes by electrons with a trajectory running parallel to a Si/SiO_2 interface. For an electron trajectory located in SiO_2, clear evidence of delocalized excitation of guided modes in Si is presented, and for an electron trajectory located in Si, an interference pattern is observed for the loss probability as a function of the distance from the interface.

II. EXPERIMENTS AND THEORY

Experiments were carried out with a monochromated FEI Tecnai F20-ST FEG-TEM equipped with a Gatan Tridiem 865ER imaging spectrometer. The full width at half maximum of the energy spread of the whole system [power supply, source spread, spectrometer, charge-coupled device (CCD)] was measured to be ~120 meV at 0.5 s acquisition time, and ~150 meV at 5 s acquisition time due to small instabilities in the high tension power supply. The use of a monochromator is essential not only in improving the energy resolution but also in giving access to the low-energy range (visible/near-infrared domain) by reducing the contributions from the tail of the zero-loss peak (ZLP). The spatial resolution corresponding to the width of the electron probe is evaluated to be between 2 and 4 nm. In order to increase the dynamic range and to prevent blooming of the CCD, an energy-selecting slit was used to block part of the intense ZLP. To increase the signal-to-noise ratio, several spectra were acquired under the same conditions and then aligned and summed (typically five to ten spectra with an acquisition time of 2–5 s). EELS experiments were performed in a scanning transmission electron miscroscope (STEM) with a convergence and acceptance semiangle of 7.5 and 6 mrad, respectively. TEM specimens were prepared by mechanical polishing along the [110] direction for the Si substrate, with 2° wedge angle. For the final polish, between 10 and 20 min of ion milling was performed. For the study at normal incidence, a slight tilt angle away from the [110] zone axis was introduced to ensure no diffraction effects were present in the EELS spectra.

To interpret the experimental spectra, a dielectric model was implemented to simulate the loss spectra. The theory is based on the Kroger's formalism[26] for the energy loss of electrons going through dielectric slabs at various incidence angles. In this model, Maxwell's equations are solved in the presence of a swift electron passing through non-magnetic media. This approach therefore includes relativistic effects such as the emission of Cherenkov and transition radiation. The loss spectra presented in this paper were obtained by integrating the loss intensity in momentum space on a plane perpendicular to the electron trajectory in a region defined by the EELS collection aperture. For normal incidence, the formalism reduces to the one presented by Kroger in an earlier paper.[20] Experimental results[3,4,10] have previously been compared to the model of Ref. 20. To account for possible oxidation of the TEM samples, Si slabs with thin SiO_2 layers on both surfaces are simulated using the formalism developed by Bolton and Chen[27] for multilayered structures. Finally, for the study of Cherenkov radiation emitted near a parallel interface, the analysis is based on the theory derived by Garcia Molina *et al.*[28] for two semi-infinite media, and the results are presented following the approach of García de Abajo *et al.*[19] Dielectric constants for Si and SiO_2 were taken from optical data tabulated in Ref. 29, and a small (10^{-4}) imaginary component was added in the band-gap region to ensure convergence of the numerical integration.

III. RESULTS AND DISCUSSIONS

The emission of guided Cherenkov modes is analyzed for three different geometries. First, for the case of an electron beam traversing a silicon slab at normal incidence, spectral features are assigned to symmetric and antisymmetric *p*-polarized modes. Then, as the sample is tilted up to 65°, changes in EELS spectra are discussed in terms of both *s*-polarized and *p*-polarized modes, and by accounting for Cherenkov radiation escaping the Si slab. Finally, an interference effect arising from a Si/SiO_2 interface running parallel to the trajectory of the incident electrons is presented, along with the possibility of delocalized excitation of guided modes.

A. Normal Incidence

The sketch presented in Fig. 1(a) illustrates a simplified ray diagram of Cherenkov radiation emitted in a silicon slab at a characteristic angle θ_c. As can be seen on the diagram, the Cherenkov angle corresponds to the incidence angle at the slab surface, and if it exceeds the threshold θ_r for total internal reflection, then the emitted light is expected to be confined in the slab. For a silicon slab in vacuum, and 200 keV electrons, the Cherenkov angle is $\theta_c \sim 67°$ (for 1.5 eV radiation), which is above the threshold for total internal reflection ($\theta_r \sim 16°$), so coupling to waveguide modes is expected.

Two experimental spectra acquired in slabs of crystalline Si are displayed in Fig. 1(b). These spectra were acquired on the same wedged sample, but at two different thicknesses. Since the wedge angle was only 2°, its effect can be neglected and the results are treated as two separate Si slabs. Below the direct electronic transition at 3.4 eV, strong features associated with radiative losses appear in the spectra. In this energy range the Cherenkov condition is satisfied ($v > c/n$, where for 200 keV electrons $v = 0.69c$). At very low energies, contributions from the ZLP tails are observed in both experimental spectra. For the thicker slab, some features are visible even below the indirect Si gap onset at 1.1 eV. For the thinner slab low-energy modes, which have higher wavelengths, are not supported, and the first main peak is observed at higher energy.

Simulation results based on Kroger's formalism[26] are presented in Fig. 1(b) and are found to accurately reproduce the observed spectra below 6 eV. To account for possible oxidation at sample surfaces, which affect the spectra at higher energies, a model with two SiO_2 layers (2 nm) at each surface was considered. For this layered structure, the model derived by Bolton and Chen[27] was implemented and the results are displayed as dotted lines in Fig. 1(b). Three main conclusions can be reached with this approach: the guided

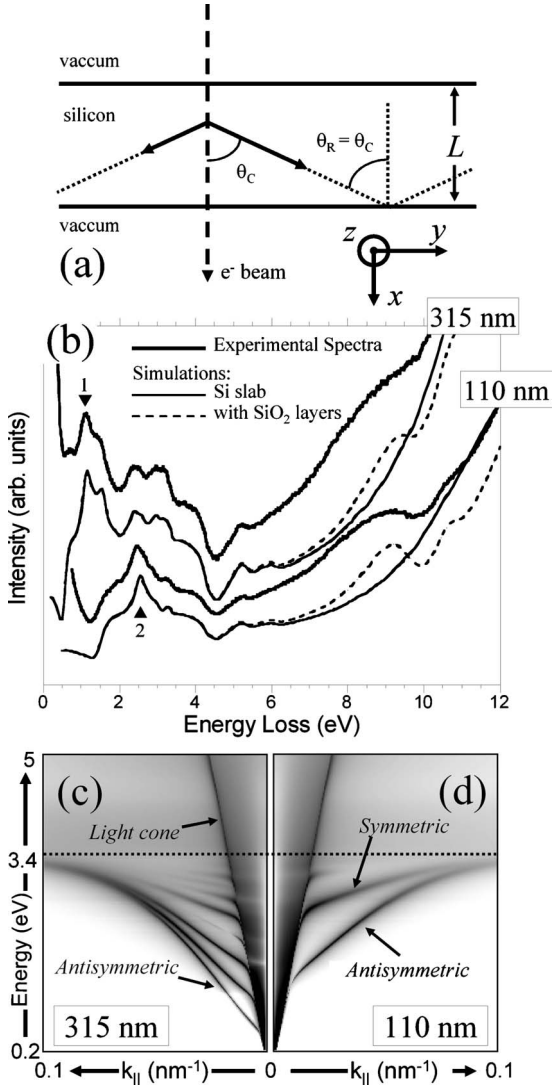

FIG. 1. (a) Simplified schematic representation of Cherenkov emission in a silicon slab. (b) Experimental and modeled spectra for silicon slabs with thicknesses of 315 and 100 nm. Simulated maps displaying the loss probability as a function of the energy (vertical axis) and the scattering vector (horizontal axis) are shown for thicknesses of (c) 315 and (d) 110 nm. On the maps, positive contributions appear dark.

modes are not affected by the presence of surface oxide layers; a change in the interface plasmon energy and intensity produces a strong feature at 8.5 eV and a weak contribution from the excitons in SiO_2 appears in the spectra at 10.5 eV just above the expected SiO_2 band-gap energy. All three predictions are confirmed experimentally.

To understand the origin of the observed radiative features, Figs. 1(c) and 1(d) present calculated loss images for the two slab thicknesses of 315 and 110 nm. These maps display the loss probability as a function of the energy (vertical axis) and the scattering vector $k_{||}$ parallel to the slab's surface (horizontal axis), which relates directly to the scattering angle of the incident electrons. The contrast on the maps is reversed and positive contributions to the loss spectra correspond to black areas. Only scattering angles much lower than the collection angle defined by the EELS aperture are presented, and no oxide layers were introduced. Two distinct areas in the images are delimited by the light cone, corresponding to the dispersion of photons in vacuum ($\omega/k=c$), where $\hbar\omega$ is the energy loss and k is the scattering vector. Contributions along the cone's edge originate from surface plasmons that display a strong dispersion in that range of scattering angles. Excitations contained inside the light cone ($k<\omega/c$) are associated in part with transition radiation, which propagates outside the sample. This emission is found not to produce strong features in loss spectra. Individual waveguide modes appear clearly outside the light cone. If a medium had a refractive index that did not vary with energy, the waveguide modes would converge towards the medium's light cone ($\omega/k=c/n$). However, in silicon, these modes are found to attenuate and disperse strongly near the direct interband transition at 3.4 eV (horizontal dotted line) and they start broadening above the Si indirect gap at 1.1 eV due to absorption.

At normal incidence, only p-polarized modes are excited. The lowest energy mode, in both Figs. 1(c) and 1(d), corresponds to an antisymmetric mode (i.e., the (yz) component of the electric field is antisymmetric about a plane cutting through the middle of the slab, see definition in Ref. 27). The first antisymmetric modes do not have a frequency threshold. All other modes have a threshold located on the edge of the light cone. The first peaks observed in the experimental spectra [labeled 1 and 2 in Fig. 1(b)] are located at energy slightly higher than the thresholds for the first symmetric modes. The broad shoulder preceding these peaks originates from the first antisymmetric modes. For a thicker slab, thresholds shift to lower energies, resulting in higher number of modes observed in the spectra, and a shift of the first peak to lower energy loss.

B. Oblique Incidence

As the slab is tilted with respect to the electron trajectory, the angle between the emitted radiation and the slab surface will vary [Fig. 2(a)]. In such a configuration, the guided modes will be different for propagation along the positive and negative k_y directions, as well as in the k_z directions. A reanalysis of the experimental loss spectra is needed to account for this break in symmetry.

Figures 2(b) and 2(c) presents two sets of experimental (top) and modeled (bottom) spectra for three tilt angles. The slab thicknesses are (b) 115 and (c) 200 nm. The observed increase in intensity for higher incidence angle can be explained by the longer path traveled by the electrons in silicon. This trend along with the general change in the shape of the spectra is well reproduced by the theory. However, several strong peaks predicted by the model appear damped in the experimental spectra, especially when the sample is tilted at 65°. To explain these results, a separate look at the modes propagating along k_y and k_z will be presented. For the following analysis based on the dielectric model, the loss maps are displayed along the (yz) plane parallel to the slab surfaces, whereas the spectra were obtained by integrating the loss signal in the detector plane (y',z') whose normal is the incident electron's trajectory.

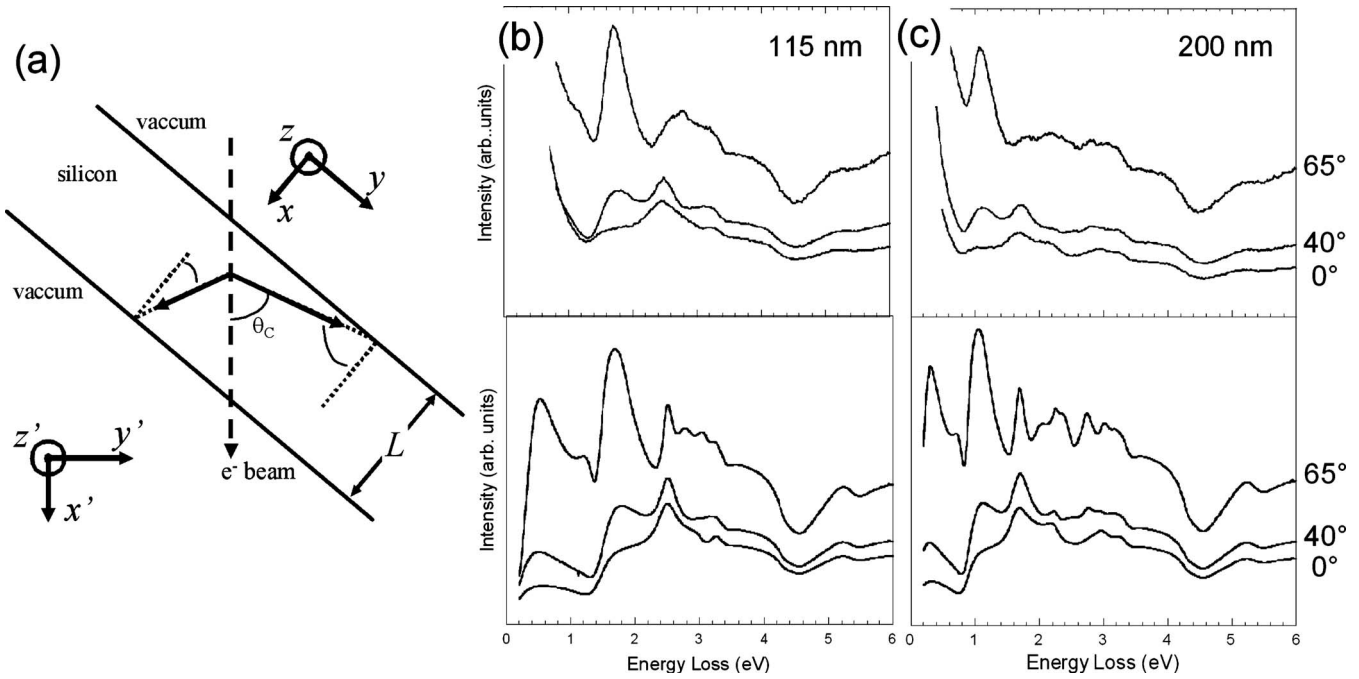

FIG. 2. (a) Simplified schematic representation of Cherenkov emission in a silicon slab tilted with respect to the electron trajectory. Experimental (top) and modeled (bottom) spectra for silicon slabs with thicknesses of (b) 115 and (c) 200 nm and for tilt angles of 0°, 40°, and 65°.

All modes propagating along k_y are found to be p polarized. Loss maps for a slab thickness of 200 nm, shown in Fig. 3 for (a) 0°, (b) 40°, and (c) 65°, reveal that the dispersion of the k_y modes remains the same, but the intensity along each line varies. As expected, the maps also display an asymmetry along the positive and negative direction, where a higher loss signal is obtained for the positive direction, in particular, for the interface plasmon (intensity close to the light cone). From the ray diagram of Fig. 2(a), it is expected that the condition for total internal reflection will no longer be satisfied in the negative direction for tilt angles higher than ~50°. At 65°, the loss image of Fig. 3(c) clearly shows a strong Cherenkov contribution inside the light cone, indicating that some radiation is no longer confined and escape the slab.

Along the tilting axis (k_z), loss images are symmetrical along the positive and negative directions. When the sample is tilted, and the electrons arrive at oblique incidence, s-polarized modes will be emitted along k_z. Figure 4(a) presents a loss image along k_z for a 200-nm-thick silicon slab tilted at 65°. In contrast to Fig. 3(c), a higher number of modes is observed since both s- and p-polarized modes are present. In the Kroger's dielectric model, the local approximation allows for the separation of the loss signal into two terms: the first being the bulk term, and the second the so-called surface term that takes into account the boundary conditions. By displaying the surface term for both s- and p-polarized modes separately, as in Figs. 4(b) and 4(c), each mode can be directly assigned to a polarization. Moreover, from the surface dispersion relations obtained from Kroger's model, the lowest energy s-polarized mode is identified as symmetric, whereas the lowest energy p-polarized mode is identified as anti-symmetric. The white lines appearing in Figs. 4(b) and 4(c) are negative contributions to cancel the Cherenkov contribution in the bulk component of the equation (see Ref. 26). Also, interface plasmon-polariton modes are p polarized, and this explains why the contour of the light cone is not as well defined in the s-polarized loss image. For 65°, as demonstrated in Fig. 4, s-polarized modes dominate along the k_z direction and are also found to contribute at lower energies.

By applying the concepts discussed above, various contributions to the experimental loss spectra can be decoupled. Figure 5 displays a comparison between the (A) experimental and (B) the modeled spectra for slab thicknesses of (a) 115 and (b) 200 nm, and for an incidence angle of 65°. Integrating the s- and p-polarized surface terms separately (C) indicates that the total s-polarized contribution is non-negligible for high tilt angles and affects the shape of the loss spectra. Furthermore, the s-polarized signal is especially high at energies below ~0.5 eV, a region difficult to study experimentally due to the presence of the ZLP tail. An evaluation of the contribution of light escaping the Si slab can be obtained by integrating the loss signal inside the light cone (D). With this approach, several prominent peaks are identified. These features are damped in the experimental spectra, especially the peaks at 2.5 eV in (a) and 1.7 eV in (b). Some factors neglected in the dielectric model, such as the wedge angle of the specimen or the electron beam convergence angle could possibly explain such discrepancies. Overall, the agreement between the theory and the experiment is sufficient to allow for the various contributions to be identified.

C. Parallel Incidence near a Si/SiO_2 interface

For an electron traversing a Si slab near a parallel interface with a SiO_2 medium, as sketched in Fig. 6(a), the guided

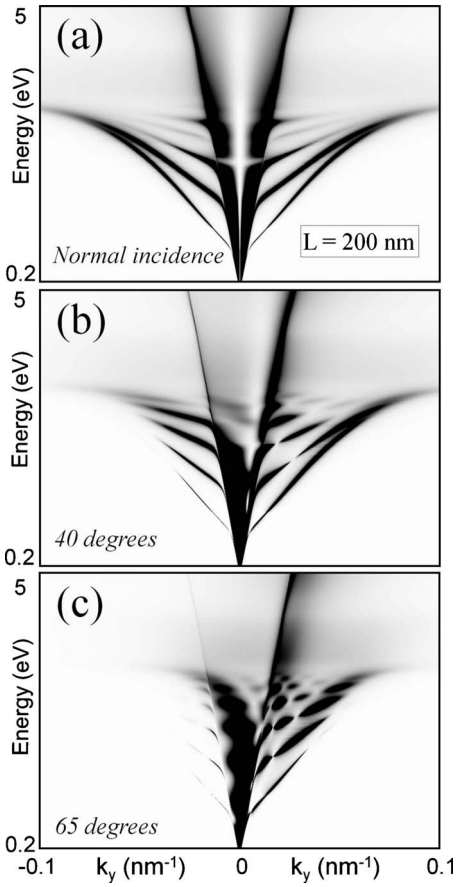

FIG. 3. Simulated maps displaying the loss probability as a function of the energy (vertical axis) and the scattering vector along the y direction (horizontal axis) for an incidence angle of (a) 0°, (b) 40°, and (c) 65°. The breaking of cylindrical symmetry as a result of tilting results in an inequivalence between $+k_y$ and $-k_y$. The slab thickness is 200 nm.

modes emitted will be affected by an extra boundary condition. Figure 6(b) displays a series of spectra acquired in Si with a sub-4 nm probe at various distance from the interface with a thick (500 nm) SiO_2 film. The thickness of the Si slab in this case is 280 nm. As the impact parameter y_0 decreases, the intensity maximum in the spectra shifts to higher energy loss, indicating that the modes with longer wavelengths are partially suppressed. For an impact parameter comparable to or greater than the slab thickness, loss spectra are close to what is expected in the absence of a Si/SiO_2 interface.

To better display the expected interference effects, experimental loss functions are displayed in Fig. 7(a) in the same way as the calculations shown in Fig. 1 of Ref. 19. The horizontal axis $Q_\perp y_0$ is a dimensionless product of the impact parameter y_0 and the momentum $Q_\perp$ for the light perpendicular to the trajectory. $Q_\perp$ is given by $(\omega/c)\sqrt{\varepsilon - c^2/v^2}$, where $\hbar\omega$ corresponds to the energy loss and ε is the energy dependant dielectric constant taken from optical data.[29] For Fig. 7(a), the imaginary part of the dielectric constant was neglected, and only the section between 0.65 and 3.3 eV of the experimental loss spectra was considered. With a $Q_\perp y_0$ scaling, multiple spectra can be displayed on the same graph. In this case, spectra acquired at impact parameters between

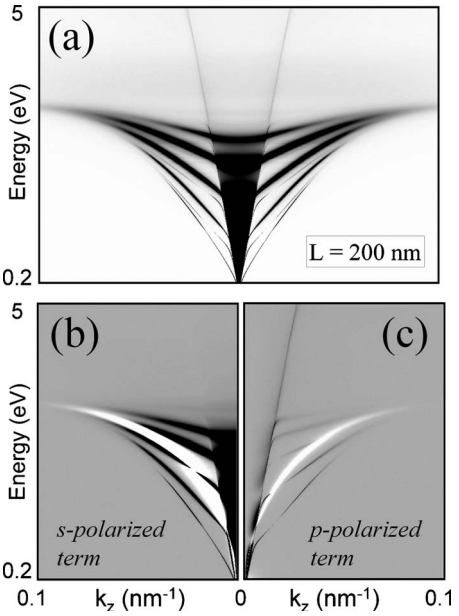

FIG. 4. (a) A simulated map displaying the loss probability as a function of the energy (vertical axis) and the scattering vector along the z direction (horizontal axis) for an incidence angle of 65° and for a slab thickness of 200 nm. The surface terms for (b) s-polarized and (c) p-polarized modes are shown separately.

40 and 125 nm (shown in Fig. 6) are all included in Fig. 7(a). The loss probability (the vertical axis) was normalized with a spectrum acquired at $y_0 = 253$ nm, which is essentially a spectrum acquired in the absence of a Si/SiO_2 interface.

From a relativistic model developed by Garcia Molina *et al.*[28] for two semi-infinite media, a clear oscillating pattern with diminishing amplitude is expected [Fig. 7(b)], as previously discussed by García de Abajo *et al.*[19] This behavior is partially reproduced in the experimental results. At low $Q_\perp y_0$, disagreements between experimental and theoretical results arise from contribution of the ZLP tail, which was not included in the model. On the experimental curves, three maxima fall near the predicted $Q_\perp y_0$ values; however, the amplitudes of the oscillations differ from the ones predicted by the model. A model that includes the finite slab thickness would be required for a more thorough analysis. Qualitatively, the oscillating behavior can also be observed directly on the series of spectra in Fig. 6. For instance, the peak at ~2.4 eV is found to increase and then decrease in intensity as the electron probe moves away from the Si/SiO_2 interface.

Finally, we consider a beam traveling in SiO_2 close to Si. Figure 8 compares two spectra taken in SiO_2 at 5 and 16 nm from the interface with a spectrum acquired in Si at 50 nm from the interface. In this case, the slab was thinner (145 nm) in order to get a better signal to noise ratio. When the electron probe is in SiO_2, the exciton transition above the band-gap onset (9.9 eV) is clearly visible. Below this onset, a low emission probability of Cherenkov radiation in SiO_2 is predicted, but it does not lead to strong peaks in the spectra. Also, the Si/SiO_2 interface plasmon produces a broad feature around 8.5 eV that displays a redshift when the probe approaches the interface, as previously observed for a similar

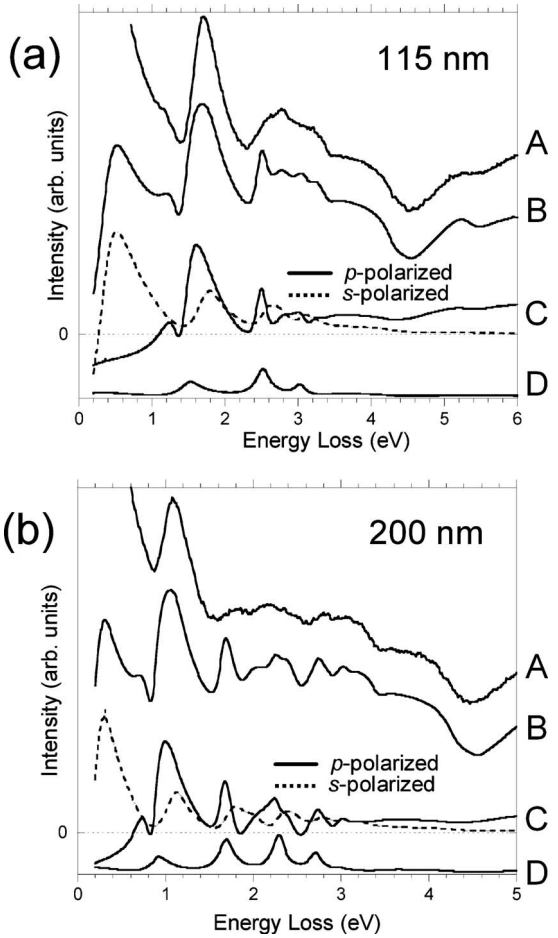

FIG. 5. (A) Experimental and (B) modeled loss spectra for an incident angle of 65° and for slab thicknesses of (a) 115 and (b) 200 nm. The integrated *s* and *p* polarized surface terms are shown separately (C), together with the integrated loss probabilities inside the light cone (D). For clarity, the D curves have been shifted downward vertically, and their zero intensity corresponds to the position of the energy-loss axes.

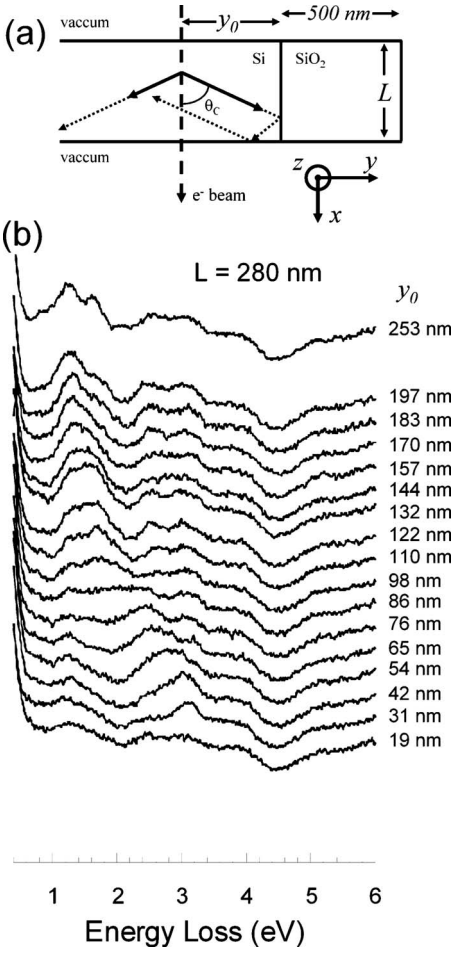

FIG. 6. (a) Simplified schematic representation of Cherenkov emission in a silicon slab in the presence of a nearby Si/SiO_2 interface. (b) A series of experimental spectra acquired at normal incidence in a 280 nm thick silicon slab at various distances y_0 from a parallel Si/SiO_2 interface. The SiO_2 layer thickness is around 500 nm.

system.[30] Interband transitions associated with the silicon slab, in particular, the direct transition above 3.4 eV, also appears even when the probe is in the SiO_2 region. Such delocalized valence excitations can dominate loss spectra when probing nanometer scale layers.[31] Below 3.4 eV, waveguide features are observed at the same energies found when the probe is located in Si. This demonstrates that Cherenkov radiation in a waveguide can also be excited by the passage of an electron in proximity, but outside of the medium. For delocalized excitations of guided modes, the loss signal decreases exponentially with the energy, reflecting the fact that higher-energy excitations are more localized.[32]

IV. SUMMARY

Boundary effects on Cherenkov radiation were studied with relativistic electrons incident on Si slabs at perpendicular and oblique incidence. The interpretation of monochromated electron energy-loss spectra acquired in a scanning transmission electron microscope with a sub-4 nm probe was based on a comparison with a local relativistic dielectric model. When the beam trajectory is perpendicular to the slab surface, *p*-polarized waveguide modes confined in Si are excited, producing well-defined features in loss spectra. The first peak appears at an energy slightly higher than the threshold for the first symmetric mode, and it follows a broad spectral feature at lower energy attributed to the first antisymmetric mode. As the slab thickness decreases, modes with higher wavelengths are suppressed, resulting in a lower number of modes being excited and a blueshift of the first peak.

Electrons traversing Si slabs at oblique incidence also couple to *s*-polarized modes, which are completely absent for the case of normal incidence. These modes propagate primarily along the direction of the tilt axis. In this configuration, new *p*-polarized modes are also excited. When the tilt angle exceeds a threshold set by the condition for total internal reflection, some Cherenkov radiation is no longer confined in the slab. Contributions from Cherenkov radiation escaping the Si slab were found to be significantly less intense than predicted, possibly due to the nonideal experimental geom-

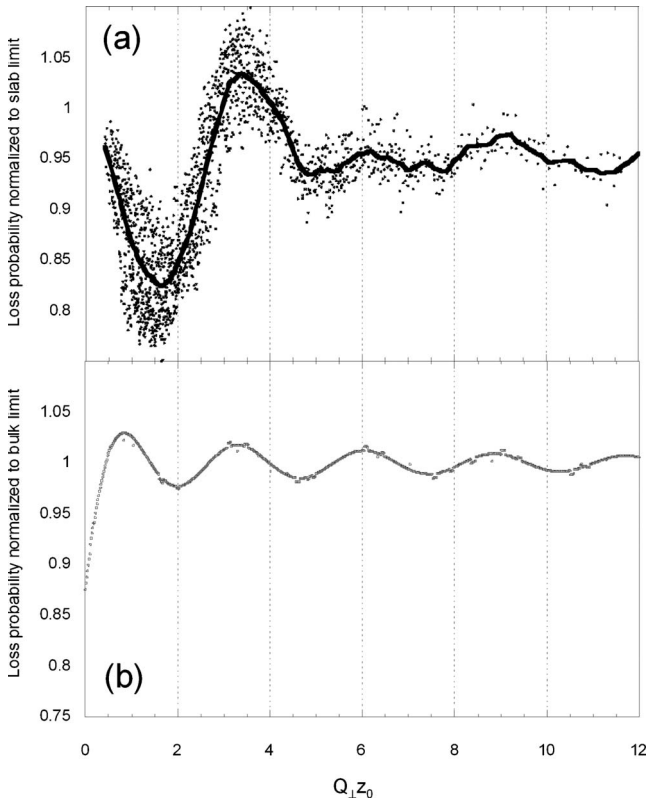

FIG. 7. (a) Loss probability as a function of $Q_\perp y_0$, where $Q_\perp$ is the momentum of the light perpendicular to the electron trajectory, as defined in Ref. 19, and y_0 is the impact parameter. Each spectra acquired at distances between 40 and 125 nm from the Si/SiO_2 interface (shown in Fig. 6) is replotted in (a) as a function of $Q_\perp y_0$ for an energy range from 0.65 to 3.3 eV, and the loss probability was normalized with a spectra acquired far (253 nm) from the Si/SiO_2 interface. The black line is an average of all the spectra. (b) Simulations for the case of two semi-infinite media. For simplicity, the Si and SiO_2 media were represented with a dielectric functions with a constant real component, which was taken at 800 nm from optical data (Ref. 29), and no imaginary component. In (b), the loss probability was normalized with the bulk limit.

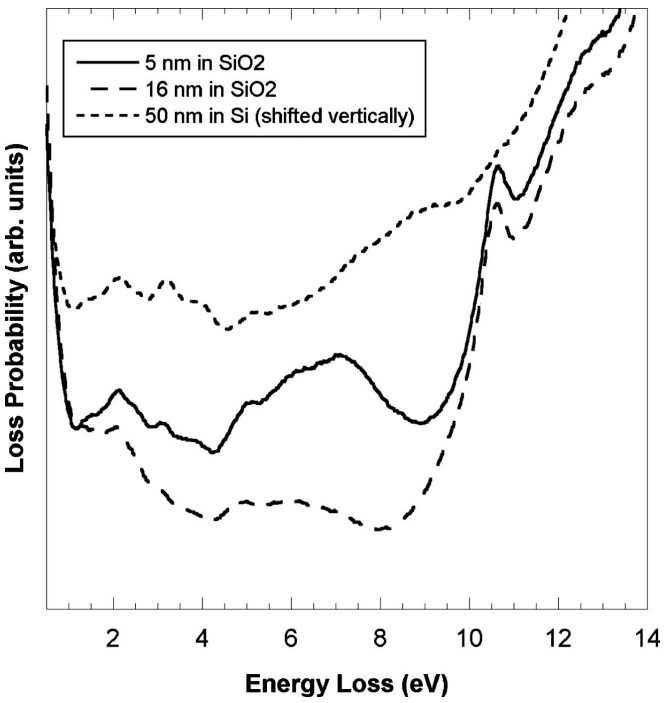

FIG. 8. Experimental spectra acquired in SiO_2 at a distance of 5 and 16 nm from the Si slab. A spectrum acquired in Si at 50 nm from the Si/SiO_2 interface is also displayed, and it has been shifted upward vertically for clarity. The slab thickness is 145 nm.

etry. Based on a comparison with a local dielectric model, the polarization and the symmetry of the modes associated with the observed spectral features were identified.

Finally, we considered the influence of a single Si/SiO_2 interface running parallel to the electron trajectory on the emission probability of guided modes in Si. When the electrons go through the Si slab, a partial suppression of the modes with longer wavelengths is observed as the electron probe approaches the Si/SiO_2 interface. An interference effect on the Cherenkov emission was identified as the source of the observed variations. For the case of an electron beam travelling in SiO_2, close to but outside the Si slab, experimental results show that a delocalized excitation of guided radiation still occurs.

In summary, the position and the incidence angle of the electron trajectory strongly affect the emission probability of guided Cherenkov radiation. As demonstrated here, monochromated electron microscopes allow for the investigation of radiative losses in a domain extending beyond the ultraviolet, covering the whole visible range and part of the near infrared. As previously derived from a dielectric theory,[25] electron energy-loss spectroscopy is related to the local photonic density of states. Thus, a combination of high spatial and energy resolution in electron energy-loss spectroscopy points to the possibility of probing optical modes over a broad spectral domain on the nanometer scale.

ACKNOWLEDGMENTS

This research was supported by the Semiconductor Research Corporation and the Cornell Center for Nanoscale Systems, an NSF NSEC. The authors are grateful to John Grazul and the Cornell Center for Materials Research, an NSF MRSEC, for technical support and maintenance of the facilities. We also thank Peter Tiemeijer and Lena Fitting Kourkoutis for help with the monochromator, and Jerome Hyun and Mathieu Kociak for useful discussions.

*Corresponding author. Present address: Brockhouse Institute for Materials Research and Canadian Centre for Electron Microscopy, McMaster University, Hamilton, ON, Canada, L8S 4L7; m.couillard@mcmaster.ca

†Present address: Physical Biology Center for Ultrafast Science and Technology, Arthur Amos Noyes Laboratory of Chemical Physics, California Institute of Technology, Pasadena, CA 91125, USA.

[1] P. A. Cherenkov, Dokl. Akad. Nauk SSSR **2**, 451 (1934).
[2] H. Raether, *Excitations of Plasmons and Interband Transitions by Electrons* (Springer-Verlag, Berlin, 1980).
[3] M. Stöger-Pollach, Micron **39**, 1092 (2008).
[4] R. Erni and N. D. Browning, Ultramicroscopy **108**, 84 (2008).
[5] L. Gu, V. Srot, W. Sigle, C. Koch, P. van Aken, F. Scholz, S. B. Thapa, C. Kirchner, M. Jetter, and M. Ruhle, Phys. Rev. B **75**, 195214 (2007).
[6] S. Lazar, G. A. Botton, and H. W. Zandbergen, Ultramicroscopy **106**, 1091 (2006).
[7] M. Stöger-Pollach, H. Franco, P. Schattschneider, S. Lazar, B. Schaffer, W. Grogger, and H. W. Zandbergen, Micron **37**, 396 (2006).
[8] M. Couillard, M. Kociak, O. Stéphan, G. A. Botton, and C. Colliex, Phys. Rev. B **76**, 165131 (2007).
[9] R. Arenal, O. Stéphan, M. Kociak, D. Taverna, A. Loiseau, and C. Colliex, Phys. Rev. Lett. **95**, 127601 (2005).
[10] A. Yurtsever, M. Couillard, and D. A. Muller, Phys. Rev. Lett. **100**, 217402 (2008).
[11] B. Schaffer, U. Hohenester, A. Trügler, and F. Hofer, Phys. Rev. B **79**, 041401 (2009).
[12] M. N'Gom, S. Li, G. Schatz, R. Erni, A. Agarwal, N. Kotov, and T. B. Norris, Phys. Rev. B **80**, 113411 (2009).
[13] W. Sigle, J. Nelayah, C. T. Koch, and P. A. van Aken, Opt. Lett. **34**, 2150 (2009).
[14] J. Nelayah, M. Kociak, O. Stéphan, F. Javier García de Abajo, M. Tencé, L. Henrard, D. Taverna, I. Pastoriza-Santos, L. M. Liz-Marzán, and C. Colliex, Nat. Phys. **3**, 348 (2007).
[15] A. Howie, Micron **34**, 121 (2003).
[16] I. Arslan, J. K. Hyun, R. Erni, M. N. Fairchild, S. D. Hersee, and D. A. Muller, Nano Lett. **9**, 4073 (2009).
[17] O. Stéphan, D. Taverna, M. Kociak, K. Suenaga, L. Henrard, and C. Colliex, Phys. Rev. B **66**, 155422 (2002).
[18] M. Kociak, O. Stéphan, L. Henrard, V. Charbois, A. Rothschild, R. Tenne, and C. Colliex, Phys. Rev. Lett. **87**, 075501 (2001).
[19] F. J. García de Abajo, A. Rivacoba, N. Zabala, and N. Yamamoto, Phys. Rev. B **69**, 155420 (2004).
[20] E. Kröger, Z. Phys. **216**, 115 (1968).
[21] C. H. Chen and J. Silcox, Phys. Rev. B **20**, 3605 (1979).
[22] C. H. Chen and J. Silcox, Phys. Rev. Lett. **35**, 390 (1975).
[23] J. K. Hyun, M. Couillard, P. Rajendran, C. M. Liddell, and D. A. Muller, Appl. Phys. Lett. **93**, 243106 (2008).
[24] F. J. García de Abajo, A. G. Pattantyus-Abraham, N. Zabala, A. Rivacoba, M. O. Wolf, and P. M. Echenique, Phys. Rev. Lett. **91**, 143902 (2003); J. J. Cha, Z. Yu, E. Smith, M. Couillard, S. Fan, and D. A. Muller, Phys. Rev. B **81**, 113102 (2010).
[25] F. J. García de Abajo and M. Kociak, Phys. Rev. Lett. **100**, 106804 (2008).
[26] E. Kröger, Z. Phys. **235**, 403 (1970).
[27] J. P. R. Bolton and M. Chen, J. Phys.: Condens. Matter **7**, 3373 (1995); **7**, 3389 (1995).
[28] R. Garcia Molina, A. Gras Marti, A. Howie, and R. H. Ritchie, J. Phys. C **18**, 5335 (1985).
[29] E. D. Palik, *Handbook of Optical Constants* (Academic, Orlando, 1998).
[30] P. Moreau, N. Brun, C. A. Walsh, C. Colliex, and A. Howie, Phys. Rev. B **56**, 6774 (1997).
[31] M. Couillard, A. Yurtsever, and D. A. Muller, Phys. Rev. B **77**, 085318 (2008).
[32] D. A. Muller and J. Silcox, Ultramicroscopy **59**, 195 (1995).